PROCEEDINGS OF 1995 IEEE INTERNATIONAL CONFERENCE ON

ROBOTICS AND AUTOMATION

Nagoya Congress Center
May 21-27,1995 Nagoya, Aichi, Japan

VOLUME 1
OF 3

Sponsored by

Science Council of Japan
The Robotics Society of Japan
The Society of Instrument and Control Engineers
The Japan Society of Mechanical Engineers
The IEEE Robotics and Automation Society

Council for Conference Organization

Aichi Prefectural Government
City of Nagoya
Nagoya Chamber of Commerce & Industry
Chubu Economic Federation
Nagoya Industrial Science Research Institute
The Chubu Industrial Advancement Center
The Foundation of Chubu Science & Technology Center
Nagoya Convention & Visitors Bureau

IEEE Catalog Number : 95CH3461-1
ISBN : 0-7803-1965-6 (Softbound Edition)
0-7803-1966-4 (Casebound Edition)
0-7803-1967-2 (Microfiche Edition)
Library of Congress Number: 90-640158

3-D Active Antenna for Contact Sensing

Makoto Kaneko, Naoki Kanayama, and Toshio Tsuji

Industrial and Systems Engineering
Hiroshima University
Higashi-Hiroshima 724 JAPAN

Abstract

This paper discusses a 3-D Active Antenna that can detect the contact location between an insensitive flexible beam and a 3-D environment through the measurement of the rotational compliance of the beam in contact with the environment. The lateral slip, which possibly occurs for the 3D Active Antenna, overestimates the rotational compliance, and as a result, brings a large sensing error for the localizing contact point. The goal of this paper is to find the contact point under such conditions. In the first step, we push the antenna to the environment. If no lateral slip is detected during this motion, the contact point can be obtained through a similar method used for the 2D model. If a lateral slip is confirmed, the pushing direction is changed continuously until we finally avoid the development of any lateral slip. We explore how to detect a lateral slip and how to determine the new pushing direction to avoid it. We show an algorithm which can search not only the contact distance but also the normal direction of the environment's surface, even under the appearance of a lateral slip during the first step. The basic idea is also verified by experiments.

I. Introduction

Active Antenna is a new sensing system enabling us to detect the contact location through the measurement of the rotational compliance of an insensitive antenna in contact with an environment. In our former work, we have shown that for a planar type Active Antenna, the contact location is a function of the rotational compliance alone, and that one active motion is necessary and sufficient for localizing the contact point irrespective to friction at the point of contact, if the straight beam is utilized [1], [2]. A big advantage of Active Antenna is that a contact point is obtained through a surprisingly simple active motion, while sophisticated active motions should be prepared for most of contact sensing to avoid a large interaction force between sensor and environment. This is because the flexibility of the antenna successfully relaxes the contact force by itself, even under a large positional error.

This work is an extended version of our former works. In this paper, we assume that the antenna can sweep in 3D space. The sensing system is composed of an insensitive flexible beam, two actuators to move the beam in 3D space, two position sensors to measure the actuator position, and a two-axis moment sensor to evaluate the contact force, while the planar model is simply composed of one actuator, one position sensor and one-axis moment sensor in addition to an insensitive flexible beam. In the 2D Active Antenna, we implicitly assumed that the antenna never makes a slip in the lateral direction, while a longitudinal slip inevitably occurs to satisfy the geometrical relationship between the antenna shapes before and after a bending deformation. The lateral slip (see Fig.1), which is the inherent characteristic for 3D Active Antenna, strongly depends on the direction of pushing, the friction at the point of contact, and the normal surface of the environment where the antenna makes contact. Generally, such a lateral slip overestimates the rotational compliance of the antenna which is in contact with the environment, and as a result, deteriorates the sensing accuracy directly, while the longitudinal slip brings a minor error only. Our goal in this paper is to find the contact location between the antenna and the environment under these conditions.

At the beginning of sensing, the antenna approaches an environment until it makes contact. Since this approach phase is exactly the same as the one discussed in other tactile based active sensing [3], we do not focus on the approach phase in this paper. Thus, we suppose that at the initial state, the antenna is already in contact with the environment. In the first active motion, we simply push the antenna to the environment. During this, a lateral slip may occur, which can be detected by the two-axis moment sensor. One of the key issues in this paper is how to detect the lateral slip by using the sensors implemented. If no lateral slip is confirmed

IEEE International Conference
on Robotics and Automation
0-7803-1965-6/95 $4.00 ©1995 IEEE

during the first active motion, the contact point can be obtained through the rotational compliance without any further active motion, because it is guaranteed that the contact location is a function of the rotational compliance alone when there is no lateral slip. Once any lateral slip is detected, however, one active motion is no longer sufficient and more than two active motions are necessary for localizing the contact point. This is because the compliance is no longer the function of the contact point alone, and varies according to how much and which direction the lateral slip occurs. The basic idea taken in the paper is to eventually find the direction that avoids any lateral slip based on the sensor information collected during the active motions. Thus, another important issue of this paper is to explore the sensing algorithm that can finally reach the pushing direction and avoid any lateral slip.

II. Related Works

A simple flexible beam sensor can take the form of a short length of spring piano wire or hypodermic tubing anchored at the end. When the free end touches an external object, the wire bends. This can be sensed by a piezoelectric element or by a simple switch [4]. A more elaborate sensor is described by Wang and Will [5]. Long antennae-like whisker sensors were mounted on the SRI mobile robot, Shakey [6], and on Rodney Brook's six-legged robot insects [7]. Hirose, et. al. discussed the utilization of whisker sensors in legged robots [8]. The sensor system is composed of an electrode and a whisker whose end is fixed at the base. This sensor unit has been arranged in an array around each foot of the legged robot, Titan III, so that it can monitor the separation between each foot and the ground to allow deceleration of the foot before contact. This sensor is also conveniently used to confirm which part of the foot is in contact with the ground. Similarly shaped whiskers have been considered for legs of the Ohio State University active suspension vehicle [9]. Russell has developed a sensor array [10] by mounting whisker sensors on a mobile robot, and succeeded in reconstructing the shape of a convex object followed by the whisker. In his work, it is assumed that the whisker tip is always in contact with the environment, and that when the whisker contacts the environment except for the tip, it is assigned to a failure mode. The major difference between previous works [4]-[10] and ours is that the Active Antenna enables us to localize a contact point between the beam and the environment, while previous works do not.

III. Basic Structure and Working Principle of 3D Active Antenna

3.1 Basic Structure

Fig.1 shows an overview of the 3D Active Antenna and its coordinate system, where Σ_B (or upper script "B") and Σ_S (or upper script "s") denote the base coordinate system and the sensor coordinate system, respectively. The 3D Active Antenna is composed of an insensitive flexible beam, two actuators to move the beam in 3D space, two position sensors to measure the angular displacements ϕ_1 and ϕ_2, and a two-axis moment sensor to detect moments around both x_s and z_s axes. The moment sensor is designed so that each sensing axis can intersect with the center of rotation (the origin of the sensor coordinate system). Now, let us define the sensing plane Π, with the plane spanned by two unit vectors whose directions coincide with x_s and y_s. The design orientation taken for the two-axis moment sensor enables us to evaluate the direction of the contact force projected on the plane Π from the outputs of the moment sensor. As a result, it allows us to examine the appearance of a lateral slip by checking the angle between the pushing direction and contact force, which will be discussed in section IV. Fig.2 shows an overview of the developed 3D Active Antenna which is composed of two DC servo motors, and a piano wire with the length of 210 mm and diameter of 0.8 mm, and a two-axis moment sensor.

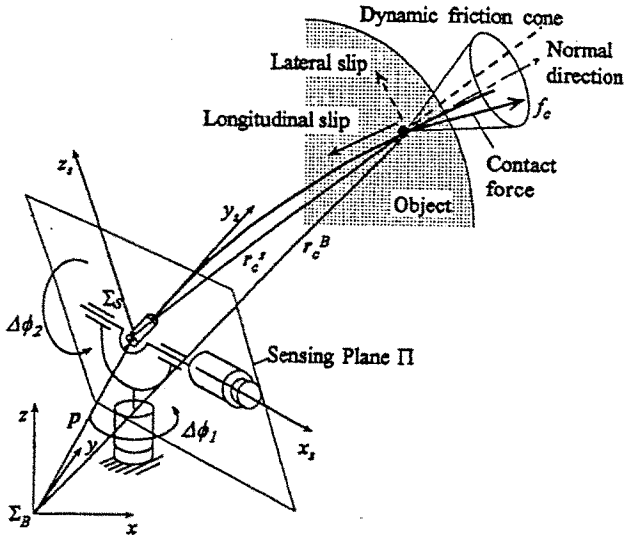

Fig.1 Basic structure and its coordinate system of 3D Active Antenna

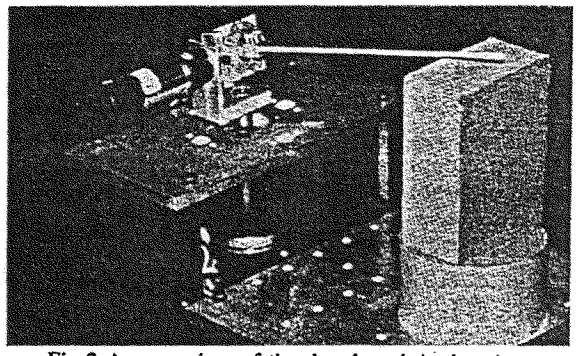

Fig.2 An overview of the developed Active Antenna

3.2 Main assumptions

For simplifying our discussions, we set the following assumptions:

Assumption 1: The antenna has equal compliance in a plane perpendicular to the longitudinal axis.
Assumption 2: The antenna deformation is small enough to ensure that we can apply a linear approximation.
Assumption 3: The shift of the contact point on the environment is negligibly small during active motions.
Assumption 4: The compliance of the environment is sufficiently small compared with that of the antenna.
Assumption 5: Before applying an active motion, the antenna is already in contact with an environment with zero force.

3.3 Basic Working Principle Without Any Lateral Slip

We have the following kinematic relationship between r_c^s and r_c^B:

$$\begin{bmatrix} r_c^B \\ 1 \end{bmatrix} = H \begin{bmatrix} r_c^s \\ 1 \end{bmatrix}, \tag{1}$$

$$H = \begin{bmatrix} R & p \\ 0_{1\times3} & 1 \end{bmatrix}, \tag{2}$$

where R and H are, respectively, the rotational matrix and the homogeneous transformation matrix representing both position and orientation of the sensor coordinate system with respect to the base coordinate system, and $0_{1\times3}=[0,0,0]$, and $p=[p_x, p_y, p_z]^t$, respectively. Since we can shift the origin of Σ_B to Σ_s without losing any generality, hereafter, we set $p=[0, 0, 0]^t$ for simplicity. Then, eq.(1) can be simply expressed by the following form:

$$r_c^B = R r_c^s. \tag{3}$$

Let $r_c^s=[0, y_0, 0]^t$ be the contact point in Σ_s with the joint angles of ϕ_1 and ϕ_2 before imparting $\Delta\phi_1$ and $\Delta\phi_2$. Once y_0 is detected, the contact point in Σ_B can be easily obtained by using the transformation matrix R between Σ_O and Σ_S. Thus, the main issue from now on is how to detect y_0. Let $r_c^{s+\Delta}$ be the position vector pointing to the contact point with respect to the new sensor coordinate system after imparting small angular displacements $\Delta\phi_1$ and $\Delta\phi_2$. The upper subscript "s+Δ" denotes the parameter taken with respect to the new sensor coordinate system. The relationship between $r_c^{s+\Delta}$ and r_c^s is given by

$$r_c^{s+\Delta} = \Delta R^t r_c^s, \tag{4}$$

For angular displacements $\Delta\phi_1$ and $\Delta\phi_2$, we have the following relationship between the moment increase $\Delta m^{s+\Delta}$ and the contact force increase $\Delta f_c^{s+\Delta}$.

$$\begin{aligned} \Delta m^{s+\Delta} &= r_c^{s+\Delta} \times \Delta f_c^{s+\Delta} \\ &= \Delta R^t r_c^s \times \Delta f_c^{s+\Delta} \end{aligned} \tag{5}$$

Taking $\Delta\phi_1 \Delta f_y^{s+\Delta} + \Delta f_z^{s+\Delta} \approx \Delta f_z^{s+\Delta}$ and $-\Delta f_x^{s+\Delta} + \Delta\phi_1 \Delta f_y^{s+\Delta} \approx -\Delta f_x^{s+\Delta}$ into consideration, we finally obtain

$$\left[\Delta m_x^{s+\Delta}\ \Delta m_y^{s+\Delta}\ \Delta m_z^{s+\Delta}\right]^t \approx y_0 \left[\ \Delta f_z^{s+\Delta}\ \ \Delta f_a^{s+\Delta}\ -\Delta f_x^{s+\Delta}\right]^t \tag{6}$$

where $\Delta f_a^{s+\Delta} = -\Delta\phi_2 \Delta f_x^{s+\Delta} + \Delta\phi_2\, \Delta f_z^{s+\Delta}$. Note that $\Delta f_a^{s+\Delta}$ is much smaller compared to the other two components. Since $\Delta m_y^{s+\Delta}$ is the moment around the longitudinal axis of the antenna, it should be small while the antenna keeps an approximate straight line. This is the reason why we do not implement the sensing axis for the moment around the y-axis. Note that the moment arm y_o is common to both moments around the x_s and z_s axes. This nature comes from the design orientation taken for the moment sensor and is conveniently used when evaluating the lateral slip at the point of contact.

Now, let us discuss the relationship between the contact force and the deformation of the antenna. The relationship between the virtual displacement vector $\Delta r_c^{s+\Delta}$ and the contact force $\Delta f_c^{s+\Delta}$ is expressed by

$$\Delta r_c^{s+\Delta} = C \Delta f_c^{s+\Delta} \tag{7}$$

where $C=\mathrm{diag}[c_0\ \varepsilon\ c_0]$, and ε is a negligibly small value since the longitudinal stiffness is extremely large compared with those of the other two directions, and c_0 is the compliance in the plane perpendicular to the longitudinal direction of the antenna. From eq.(7), picking up two components in the sensing plane, we can obtain,

$$\Delta\phi_1 y_0 \approx c_0 \frac{\Delta m_z^{s+\Delta}}{y_0} \qquad \Delta\phi_2 y_0 \approx c_0 \frac{\Delta m_x^{s+\Delta}}{y_0} \tag{8}$$

For example, if we assume a beam whose cross sectional area is circular, c_0 is given by $c_0 = y_0^3 / 3EI$, where E and I are the modulus of elasticity and the second moment of cross section of the antenna, respectively. Then, eq.(8) can be rewritten by,

$$y_0 \approx 3EI \frac{\Delta\phi_1}{\Delta m_z^{s+\Delta}} \qquad y_0 \approx 3EI \frac{\Delta\phi_2}{\Delta m_x^{s+\Delta}} \tag{9}$$

Thus, we can obtain the contact point y_0 by using either one in eq.(9). Since $\Delta\phi_1/\Delta m_z^{s+\Delta}$ and $\Delta\phi_2/\Delta m_x^{s+\Delta}$ mean the rotational compliance around the z-axis and the x-axis, respectively, eq.(9) eventually results in the following compact form:

$$y_0 \approx 3EIc \tag{10}$$

where c is the rotational compliance of the system in contact with an environment, and given by $c = \Delta\theta / \|\Delta M\|$, with $\Delta\theta = \|\Delta r_c^{s+\Delta}\| / y_0 = \sqrt{\Delta\phi_1^2 + \Delta\phi_2^2}$, $\Delta M = \sqrt{(\Delta m_z^{s+\Delta})^2 + (\Delta m_x^{s+\Delta})^2}$. Equation (10) explains the basic working principle of Active

Antenna and means that the contact distance is simply proportional to the rotational compliance which varies according to the location of contact point. Note that the location of the contact point changes linearly according to c and it is the function of c alone. These results exactly coincide with our analytical results obtained for the planar type Active Antenna [1], [2].

IV. Lateral Slip and Its Effect on Contact Sensing

Here we explain the lateral slip by using the idea of the friction cone. It should be noted that, during the sensing motion, the longitudinal slip inevitably occurs, as shown in Fig.1, because a beam-like piano wire is extremely stiff in the longitudinal direction and is a little elongated along the direction of an axial force, while it easily deforms for a bending moment. When the angular displacements, $\Delta\phi_1$ and $\Delta\phi_2$, are imparted to the antenna, it deforms while keeping contact as shown in Fig.1. If we can neglect the axial elongation of the antenna, it continuously makes a longitudinal slip on the point of contact to the environment as $\Delta\phi_1$ and $\Delta\phi_2$ increase. This allows us to consider only the case of the dynamic friction cone during the whole active motion.

Fig.3 shows the relationship among the virtual displacement vector $\Delta r_v^{s+\Delta}$, the effective displacement vector $\Delta r_e^{s+\Delta}$ and the dynamic friction cone after a pushing motion, where α is the angle of the dynamic friction cone.

Fig. 4 shows several physical parameters on the sensing plane Π, where all components are projected on the sensing plane Π and β denotes the angle between the normal direction **n** and the contact force Δf_{cs} projected on the sensing plane Π, and ν^+, ν^-, φ, ψ and λ denote outer and inner normal directions of the environment's surface, the direction of Δf_{cs}, the pushing direction with respect to the sensor coordinate system, and the pushing direction with respect to the environment surface, respectively. Since we assume the uniform compliance by assumption 1, the contact force always appears in the opposite direction against the effective displacement vector $\Delta r_e^{s+\Delta}$. This means that the contact point moves so that $\Delta r_e^{s+\Delta}$ and $\Delta f_c^{s+\Delta}$ are colinear each other. It should be noted that the force projected on the sensing plane can exist not only on the boundary but also within the dynamic friction cone, while the contact force should always exist on the boundary of dynamic friction cone. Since $\|\Delta r_v^{s+\Delta}\| > \|\Delta r_e^{s+\Delta}\|$ while under a lateral slip, $\Delta f_c^{s+\Delta}(\|\Delta r_v^{s+\Delta}\|) > \Delta f_c^{s+\Delta}(\|\Delta r_e^{s+\Delta}\|)$, which means that the contact force under no lateral slip is larger than that under one for the same $\Delta\phi_1$ and $\Delta\phi_2$. Thus, the rotational compliance is generally overestimated under a lateral slip. As a result, the sensing accuracy will be deteriorated. This is a big difference between 2D and 3D Active Antennae.

Before the analysis of the lateral slip, we make clear what physical parameters we can measure by utilizing the sensors implemented. There are two physical parameters obtained by the sensors.

(1)The direction of contact force projected on Π, ψ:
From eq. (6), the following relationship exists.

$$\frac{\Delta m_x^{s+\Delta}}{-\Delta m_z^{s+\Delta}} = \frac{\Delta f_z^{s+\Delta}}{\Delta f_x^{s+\Delta}}, \tag{11}$$

$$\beta = \tan^{-1}\left(\frac{\Delta f_z^{s+\Delta}}{\Delta f_x^{s+\Delta}}\right) = \tan^{-1}\left(\frac{\Delta m_x^{s+\Delta}}{-\Delta m_z^{s+\Delta}}\right). \tag{12}$$

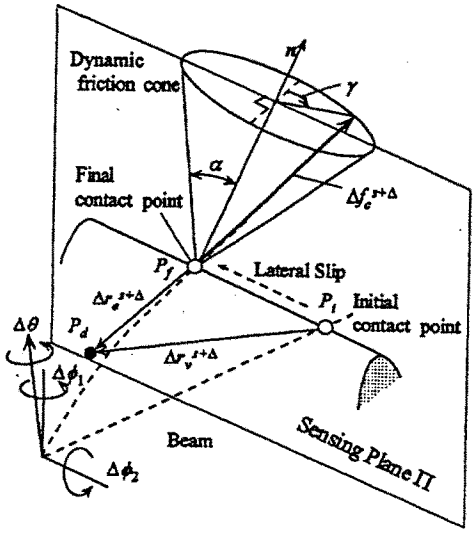

Fig.3 A general view of 3D Active Antenna when a lateral slip occurs.

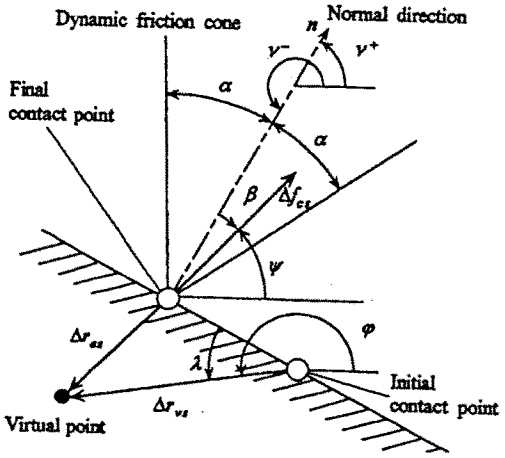

Fig.4 Notations on the sensing plane Π

Since both $\Delta m_x^{s+\Delta}$ and $\Delta m_z^{s+\Delta}$ can be measured by the moment sensor, we can obtain the direction of the contact force projected on the sensing plane Π.

(2)The pushing direction φ:

Since each actuator has position sensor, the pushing direction can also be measured.

Now, let us discuss the relationship between the pushing direction and the direction of the contact force. For a compound pushing angle $\Delta\theta$, the lateral slip s_{lat} is given by,

$$s_{lat} = y_0\Delta\theta\,(\cos\lambda - \sin\lambda\tan\beta) \tag{13}$$

From the geometrical relationship, the effective displacement vector $\Delta r_e^{s+\Delta}$ is imparted by

$$\|\Delta r_e^{s+\Delta}\| = y_0\Delta\theta\frac{\sin\lambda}{\cos\beta} \tag{14}$$

The contact point in the antenna makes a slip in the direction expressed by the ratio of the changing rate of the lateral slip $\dot{s}_{lat}$ and that of the longitudinal slip $\dot{s}_{lon}$, which eventually provides the following relationship.

$$\tan\gamma = \frac{d}{d\Delta\theta}(s_{lat}) / \frac{d}{d\Delta\theta}(s_{lon}) \tag{15}$$

Here, we assume that the changing rate of s_{lon} with respect to $\Delta\theta$ is given by the following equation.

$$\frac{d}{d\Delta\theta}(s_{lat}) = k y_0\Delta\theta\frac{\sin\lambda}{\cos\beta} \tag{16}$$

where k is a positive constant and determined by solving the load-deformation equation of the beam. Actually, the model given by eq.(16) provides a very good approximation with experimental data. Finally, considering the geometrical relationship of $\tan\beta = \tan\alpha\sin\gamma$, we obtain,

$$\tan\beta - \tan\alpha\sin\left(\tan^{-1}\left(\frac{\cos\lambda - \sin\lambda\tan\beta}{k\Delta\theta\sin\lambda/\cos\beta}\right)\right) = 0 \tag{17}$$

Considering further geometrical relationships, $\lambda = \varphi - v^+ - \pi/2$ and $\beta = v^+ - \psi$, we can obtain the following form from eq.(17).

$$\psi = g_1(\varphi, \Delta\theta, v^+, \alpha) \tag{18}$$

We can see that eq. (18) shows the input-output relationship. For a pushing motion with the pushing direction of φ and the pushing angle $\Delta\theta$ as an input, the direction of the contact force projected on the sensing plane is provided as an output. It should be noted that the output ψ includes the environment's geometry v^+ and the friction angle α at the point of contact. Our indirect goal is to find the outer normal direction v^+ through the active motion. Once v^+ is detected, then the last pushing motion to the inner normal direction will enable us to obtain the exact contact distance. So, the main question from now on is how to reach the outer normal direction v^+ through the active motion.

V. Planning of Active Motions

5.1 Case 1: No lateral slip

In this case, the analysis taken in section III remains true, and the basic working principle eventually reduces to that of a planar Active Antenna. However, a natural question that comes up is how to recognize that the lateral slip is not happening under the sensors implemented.

Let δ be the angle between the contact force and the virtual displacement vector, namely $\delta = \varphi - \psi$. When the virtual displacement and the contact force vectors are colinear to each other, the lateral slip is perfectly blocked. This condition can be confirmed by examining the index, $|\delta - \pi| = 0$. Based on $|\delta - \pi|$, it can be judged whether a lateral slip is happening or not. Once we can confirm that there is no lateral slip, the contact point can be evaluated along the idea explained in section III.

5.2 Case 2: Lateral slip

As expected from Fig.3, under a lateral slip, the virtual displacement and the contact force vectors are no more colinear to each other. This state can be confirmed by examining $|\delta - \pi| \neq 0$. It should be noted that the contact force always exists on the boundary of the dynamic friction cone during the lateral slip, as shown in Fig.3, but it is no more on the boundary when the contact force is projected on the sensing plane, as shown in Fig.4. From eq.(18), we can see that the direction ψ is a function of the pushing direction alone when the environment and the pushing angle $\Delta\theta$ are given, since both v^+ and α become constant. This relationship can be written by $\psi = g_2(\varphi)$. The direction of the contact force ψ provides us with an important clue for determining the next pushing direction. Considering that $\delta = \varphi - \psi$, eq.(18) can be rewritten in the following form.

$$\delta = \varphi - g_2(\varphi) \tag{19}$$

Since $\delta = \pi$ under no lateral slip, finding the pushing direction φ satisfying $\delta = \pi$ corresponds to avoiding any lateral slip.

To explain an example of the concrete form of the function $g_1(\varphi, \Delta\theta, v^+, \alpha)$, let us assume the pushing motion for the environment whose outer normal direction v^+ is equal to $\pi/2$ and the friction angle α to $\pi/18$. We also assume the pushing angle of $\Delta\theta = \pi/36$. Fig. 5 shows the relationship between the pushing direction φ and δ, where the real line denotes the analytical result and the circles show the experimental results. The matching between analytical and experimental results is fairly good, which suggests the validation of the analysis taken in chapter IV. The important feature is that φ is the simply increasing function with respect to δ, while we do not provide the exact proof owing to the limited number

of pages. This feature is important for ensuring the convergence of the algorithm proposed in this section. Also we would remark that δ is very close to π, when the pushing direction is so selected that it can enter the dynamic friction cone. Because of this particular feature, the compliance obtained for a pushing motion whose direction exists within the friction cone is not so different from that obtained for the normal direction.

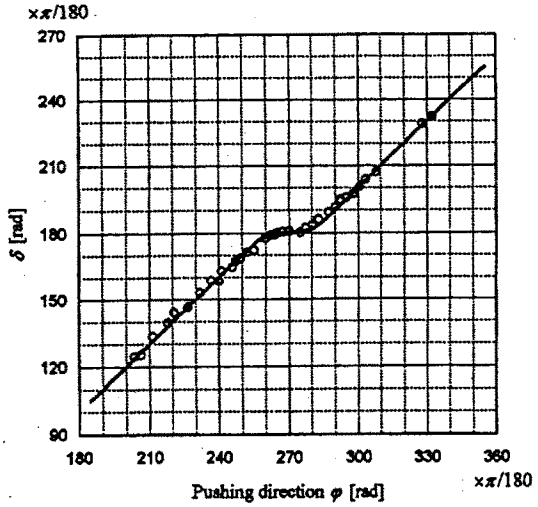

Fig.5 The relationship between δ and φ ($\alpha=\pi/18$, $\Delta\theta=\pi/36$)

[Algorithm]
1)The 1st trial: Assume the first pushing motion in an arbitrary direction $\varphi^{(1)}$ for the given environment, where the upper subscript denotes the number of trial. Let $\psi^{(1)}$ be the direction of contact force resultantly obtained for the first pushing motion.
2)The 2nd trial: The second pushing direction is chosen in the following,

$$\varphi^{(2)}=\varphi^{(1)}-\frac{\pi}{2}\mathrm{sign}(\delta^{(1)}-\pi) \tag{20}$$

where $\delta^{(1)}=\varphi^{(1)}-\psi^{(1)}$. When we choose the second pushing direction according to eq.(20), $\psi^{(1)}$ and $\psi^{(2)}$always lie in two different regions, namely, one is the right half plane with respect to the outer normal vector, and the other is the left one. Since the contact force projected on Π can never be away from the boundary of the dynamic friction cone projected on Π, the following condition hold.

$$v^+-\frac{\alpha}{2}<\frac{\psi^{(1)}+\psi^{(2)}}{2}<v^++\frac{\alpha}{2} \tag{21}$$

Eq.(21) implies that the angle between v^+ and the arithmetic mean of $\psi^{(1)}$ and $\psi^{(2)}$ is less than $\alpha/2$.

3)The 3rd trial: The third pushing direction is chosen in the following,

$$\varphi^{(3)}=(\psi^{(1)}+\psi^{(2)})/2+\pi \tag{22}$$

Because of the form of the function shown in Fig.5, $\psi^{(3)}$ (the direction of contact force) is closer to the normal direction than $\varphi^{(3)}$, namely, $|\varphi^{(3)}-v^-|>|\psi^{(3)}-v^+|$. From ineq.(21) and eq.(22), the difference between $\psi^{(3)}$ and v^+ is at most $\alpha/2$.

4)The 4th trial:
Picking up $\psi^{(3)}$ and either $\psi^{(1)}$ or $\psi^{(2)}$, we choose the fourth pushing direction in the following.

$$\varphi^{(4)}=(\psi^{(3)}+\psi^{(1|2)})/2+\pi \tag{23}$$

where $(a|b)\equiv\{x|\min(|\delta^{(x)}-\pi|), x=a, b\}$ By introducing this function, we can always choose the trial whose lateral slip is smaller than the other.

In general, for the n-th trial, we can easily prove that the following inequality exists.

$$|\psi^{(n)}-v^+|<\alpha/2^{n-2},\ n\geq 3 \tag{24}$$

Since $\lim_{n\to\infty}\{\alpha/2^{n-2}\}=0$, $\lim_{n\to\infty}\psi^{(n)}=v^+$, which means that the direction of contact force finally reaches the outer normal direction, namely, the pushing direction coincides with the inner normal direction. Thus, we can find the normal direction of the environment. Once we can detect the direction, the contact distance can be obtained through the pushing motion along the direction detected, because it is guaranteed that no lateral slip occurs.

VI. Experimental Approach

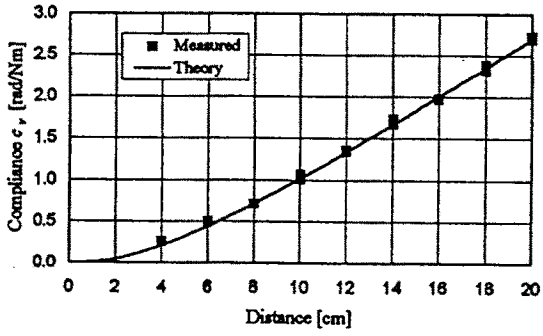

Fig.6 Calibration test without any lateral slip

The damping control is utilized for each actuator, since the antenna automatically stops with a prespecified torque, when it contacts the environment. Without any careful motion planning, the first active motion is executed automatically.

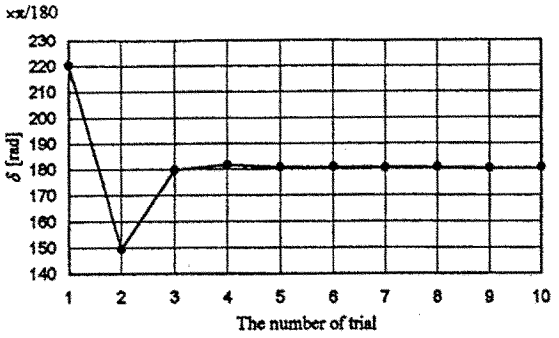

(a) δ versus the number of trial

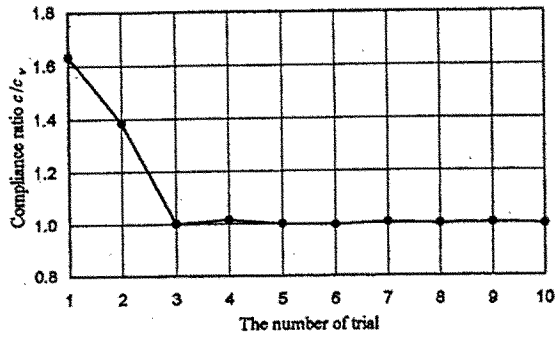

(b) c/c_v versus the number of trial

Fig.7 Convergence process for δ and c/c_v

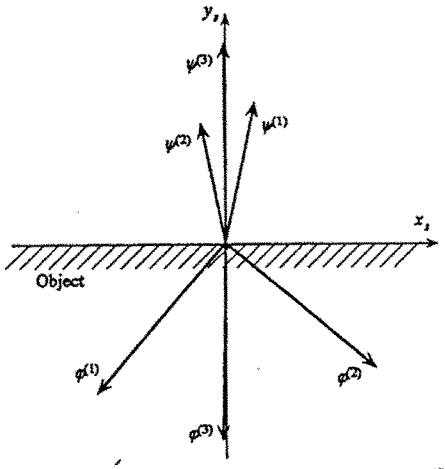

Fig.8 The relationship between $\varphi^{(i)}$ and $\psi^{(i)}$

Fig.6 shows the calibration test with five trials for each contact location with no lateral slip, where c_v denotes the rotational compliance obtained for the pushing motion against the normal direction of the environment, and the real curve corresponds to the theoretical one obtained by considering the length of the adapter. From Fig.6, we can understand that the repeatability is fairy good and the experimental data are very close to the theoretical curve.

Fig. 7 (a) and (b) show the process of convergence of δ and c/c_v with respect to the number of trial, respectively. It should be noted that both δ and c/c_v converges very quickly as the number of trial increases. With three times trials, both δ and c/c_v almost reach their equilibrium points. When c/c_v is equal to unity, we can obtain the contact distance very accurately.

Fig.8 shows the relationship between i-th pushing direction and the direction of i-th contact force. For the first pushing, the antenna makes a lateral slip toward the left side, and for the second one, it again results in failure in avoiding a lateral slip and as a result it moves toward the right side. The third pushing direction computed by eq.(22) provides nearly the inner normal direction, and, therefore, the direction of contact force is also very close to the outer normal direction.

VII. Conclusions

We explained the basic principle of 3D Active Antenna and demonstrated that the location of the contact point is simply proportional to the rotational compliance alone, if there is no lateral slip. We considered how to detect the lateral slip from the sensors available, and showed that this can be done by using the two-axis moment sensor. We further showed that even under a development of lateral slip during the first active motion, the proposed algorithm can eventually reach the pushing direction without any lateral slip, and the contact distance can be obtained with the normal direction.

References:

[1]Kaneko, M: Active Antenna, *Proc. of the 1994 IEEE Int. Conf. on Robotics and Automation*, pp2665-2671, 1994.

[2]Kaneko, M., N. Ueno, and T. Tsuji, Active Antenna (Basic Working Principle) *Proc. of the 1994 IEEE Int. Conf. on intelligent Robotics and Systems*, pp1744-1750, 1994.

[3]Kaneko, M., H. Maekawa, and K. Tanie, Active Tactile Sensing by Robotic Fingers Based on Minimum-External-Sensor-Realization, *Proc. of the 1992 IEEE Int. Conf. on Robotics and Automation*, pp1289-1294, 1992.

[4]Russell, R. A.: Closing the sensor-computer-robot control loop, *Robotics Age*, April, pp15-20, 1984.

[5]Wang, S. S. M., and P. M. Will: Sensors for computer controlled mechanical assembly, *The Industrial Robot*, March, pp9-18, 1978.

[6]McKerrow, P.: Introduction to Robotics, *Addison-Wesley*, 1990.

[7]Brooks, R. A.: A robot that walks; Emergent behaviors from a carefully evolved network, *Neural Computation*, vol.1, pp253-262, 1989.

[8]Hirose, S., et. al.: Titan III: A quadruped walking vehicle, *Proc. of the Second Int. Symp. on Robotics Research*, MIT Press, Cambridge, Massachusetts, 1985.

[9]Schiebel, E. N., H. R. Busby, K. J. Waldron: Design of a mechanical proximity sensor, Robotica, vol.4, pp221-227, 1986.

[10]Russell, R. A.: Using tactile whiskers to measure surface contours, *Proc. of the 1992 IEEE Int. Conf. on Robotics and Automation*, pp1295-1300, 1992.